ATMOSPHERIC WATER VAPOUR DETERMINATION BY THE INTEGRATION OF INSAR AND GNSS OBSERVATIONS

Fadwa Alshawaf[1, 2], Thomas Fuhrmann[2], Bernhard Heck[2], Stefan Hinz[1], Andreas Knoepfler[2], Xiaoguang Luo[2], Michael Mayer[2], Andreas Schenk[2], Antje Thiele[1], Malte Westerhaus[2]

[1] Institute of Photogrammetry and Remote Sensing (IPF), [2] Geodetic Institute Karlsruhe (GIK)
Karlsruhe Institute of Technology (KIT), D- 76131 Karlsruhe, Germany
E-mail: fadwa.alshawaf@kit.edu

ABSTRACT

High spatial and temporal variations of atmospheric water vapour cause an unknown delay on microwave signals emitted from space-borne transmitters. This delay is considered as a major error source in Interferometric Synthetic Aperture Radar (InSAR) applications as well as high-precision applications of the Global Navigation Satellite Systems (GNSS). Temporal variability of water vapour is estimated directly with a high temporal resolution from GNSS measurements. On the other hand, InSAR can provide information about the spatial variations of atmospheric water vapour. The main goal of this project is to integrate InSAR phase observations and GNSS measurements collected from sites distributed within the SAR image to derive high spatially-resolved maps of atmospheric water vapour. In this contribution research progress and first results are presented.

1. INTRODUCTION

Atmospheric water vapour is one of the most important constituents of the Earth's atmosphere and is present even in clear skies. Its significance arises from the fact that it is a primary contributor to greenhouse effect which influences the temperature average of the Earth's surface resulting in globe warming. Atmospheric water vapour is characterized by high temporal and spatial fluctuations which imposes continuous determination of its content. Conventional meteorological devices such as radiosondes and water vapour radiometers are employed for measuring atmospheric water vapour. Radiosondes provide measurements at fine vertical resolution but they are limited in observing temporal and horizontal variations of water vapour due to high costs [1]. Water vapour radiometers do not measure the fine spatial variations of water vapour and are more suitable for use over oceans [1].

Concerning space-borne systems, water vapour reduces the propagation velocity of GNSS and InSAR signals, delaying the time required to reach the ground. This effect can be exploited for sensing water vapour from space. In the past twenty years, GNSS have been used for water vapour sounding (see e.g. [1 and 2]). Due to the high temporal resolution of GNSS measurements, they enable the observation of the temporal variations of water vapour. This can be done only at sparse sites which limits the spatial resolution of water vapour maps derived based on GNSS. InSAR phase observations, however, have a tight spatial resolution over a wide coverage. Since InSAR is affected by water vapour in the same way as GNSS, it can be used to reconstruct water vapour at a finer spatial resolution. It is worth mentioning that InSAR observations are relative in time, accordingly it is necessary to retrieve absolute magnitudes.

Within this project, a combination of InSAR and GNSS is investigated for the reconstruction of water vapour. Integrated Water Vapour (IWV) content is derived from GPS measurements using the strategy of Precise Point Positioning (PPP) at the SAR overpass time. Atmospheric phase screens (APS) are extracted from InSAR interferograms using Persistent Scatterer Interferometry (PSI) [3]. Figure 1 shows an overview of the procedures for deriving water vapour content using GNSS and InSAR measurements. Meteorological observations such as air pressure and temperature are indispensable for accurate retrieval of IWV. In this study, meteorological data are received from the Weather Research and Forecasting (WRF) model [4].

2. RESEARCH AREA AND DATA SET

This research is carried out using data collected in the region of Upper Rhine Graben (URG) in Germany. This region is well covered by the homogenously distributed permanent GNSS sites [5]. InSAR interferograms are formed from seventeen co-registered ENVISAT images (100×100 km^2) of URG (zone Karlsruhe). They are observed in the time period 2003 to 2008. The images are acquired during descending passes of track 294 with a minimum of 35 days temporal baseline. The phase due to Earth's topography is removed using a Digital Elevation Model (DEM) of 5 m resolution and height accuracy of about 20 cm. GNSS measurements with a 30 seconds sampling time are received from the GNSS URG network (GURN). Meteorological data, including

Proc. 'Fringe 2011 Workshop', Frascati, Italy,
19–23 September 2011 (ESA SP-697, January 2012)

2D water vapour fields of 3×3 km^2 are received from the WRF model. Besides, surface meteorological observations are provided from meteorological stations of the German weather service (DWD). Spatial interpolations of the meteorological observations will be required. Tab. 1 summarises the properties of the data sets.

Table 1: GNSS, InSAR, WRF data utilized for atmospheric water vapour determination.

	GNSS	InSAR		WRF
System	GPS	ENVISAT	ERS- 1/2	WRF 3.1
Temporal resolution	30 sec	35 days	1 day	10 min
Spatial resolution	Site-wise	20×20 m^2	25×25 m^2	3×3 km^2
Data availability	Since 2002	2003-2008	1996	2005

3. ATMOSPHERIC PHASE SCREEN FROM INSAR

The interferometric phase for each pixel in an InSAR interferogram is given by the superposition of different contributions such as topography, Earth surface displacement, and atmosphere. Interferogram images are built from the difference between phase observations at different imaging times. Interferometric phase observed in the interferogram is written as:

$$\phi_{\text{int}} = \phi_{\text{topo}} + \phi_{\text{disp}} + \phi_{\text{atm}} + \phi_{\text{orbit}} + \phi_{\text{flat}} + \phi_{\text{noise}} \quad (1)$$

where ϕ_{topo} is the topographic phase component. ϕ_{disp} is the phase component due to the Earth surface displacement between the two SAR acquisitions. ϕ_{atm} is defined as differential phase shift caused by the propagation of the signal through the atmosphere. The phase component due to the inaccuracy of satellite orbit is given by ϕ_{orbit} and ϕ_{flat} is the phase component due to the Earth curvature. ϕ_{noise} is mainly due to the system thermal noise and the loss of coherence between the two observations. The relation between the path delay along the radar line-of-site and the atmospheric phase is given by the following relation:

$$\text{STD} = \frac{\lambda}{4\pi}\phi_{\text{atm}} \quad (2)$$

STD is the slant total delay in mm. λ is the radar wavelength. The STD can be mapped to the vertical direction as follows:

$$\text{ZTD} = \text{STD} \cdot \cos\theta_{\text{inc}} \quad (3)$$

ZTD is the zenith total delay, and θ_{inc} is the radar incidence angle. This relation has been commonly used in [6, 7, and 8]. One should consider the uncertainty fraction in this relation due to the special radar geometry. The ZTD is considered as the sum of the delay due to the dry gases known as zenith dry delay (ZDD) and the delay due to water vapour called zenith wet delay (ZWD). The delay can then be translated into

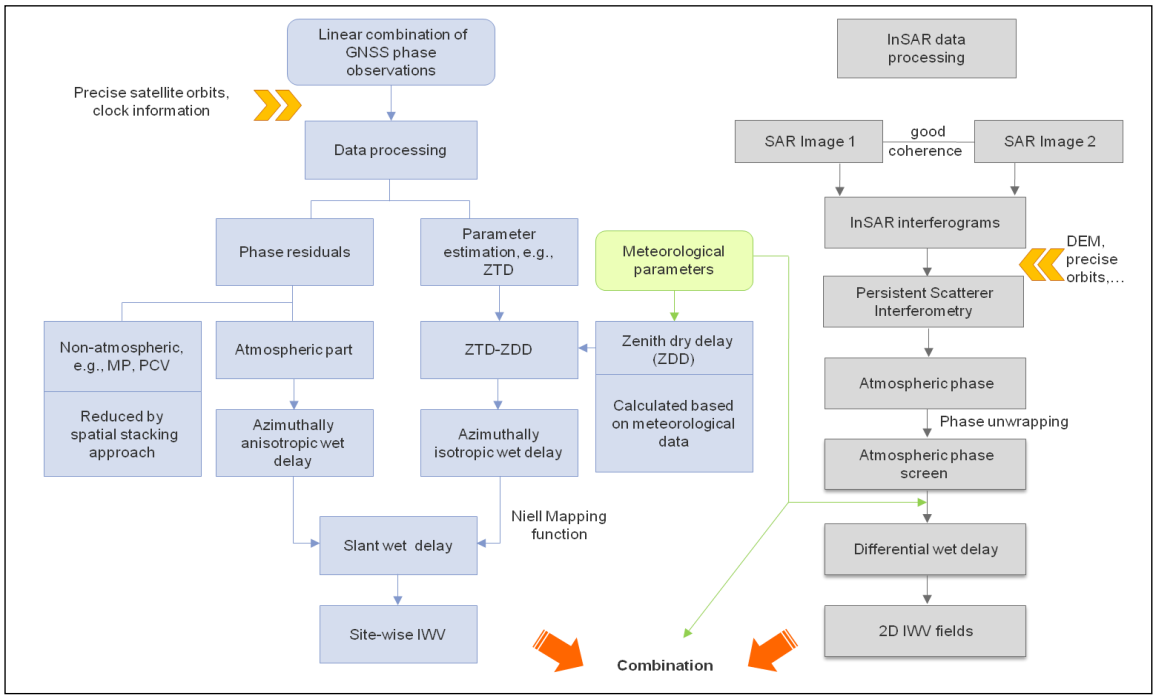

Figure 1: Deriving IWV content from InSAR and GNSS measurements. Meteorological observations are indispensable.

IWV (mm) values using the following relation:

$$\mathrm{IWV} = \Pi \cdot \mathrm{ZWD} \qquad (4)$$

Π is a constant calculated empirically based on air temperature [9].

InSAR interferograms are formed from seventeen the co-registered images. Topographic phase component is removed based on a reference DEM. PSI, particularly Stanford Method for Persistent Scatterers (StaMPS [3]), is applied to the image stack for retrieving APS maps from the interferograms. Separating the displacement phase component from InSAR interferograms may pose a challenge depending on the surface motion in the test area. In URG area shown in Fig. 2, however, only very small long-term tectonic motions were observed which can be, reasonably, assumed negligible. The remaining phase is processed to retrieve the atmospheric phase component observed in each interferogram.

Due to the fact that the signal delay caused by dry gases varies slowly in time and space, it is most likely that its effect is eliminated through the interferometric processing. Therefore, the APS contains contributions mainly due to water vapour (called wet delay). The slant delay is calculated from the phase using Eq. 2. Fig. 2 shows two APS maps (converted to mm) extracted using PS InSAR. Forest areas are almost empty of PS points; therefore, interpolations in space are performed

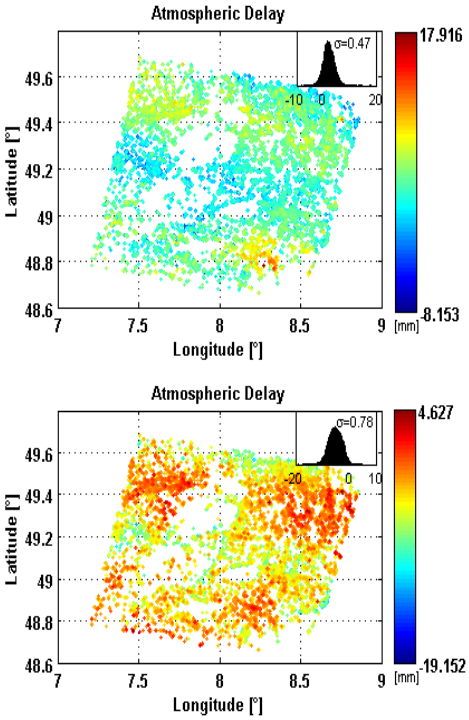

Figure 2: SWD retrieved from InSAR by applying PSI. The master image is acquired on 27062005; one slave image is acquired on 08012007 (upper) and the other on 01082005 (lower). The histograms exhibit more variations of the atmospheric signal during summer.

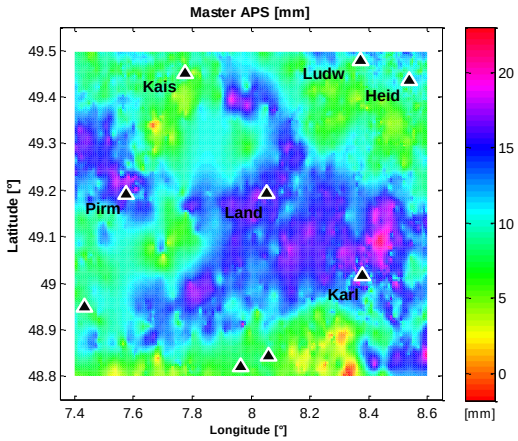

Figure 3: Master APS (in mm) extracted by applying PSI on ENVISAT image stack (long trends are removed). Spatial interpolations are obtained by means of kriging. Black triangles show the location of the GNSS sites

by means of ordinary kriging [10]. This is possible since the atmospheric signal is spatially correlated and the density of the PS points is 11 points/km^2.

The atmospheric phase appeared in the master image (acquired on 2005-06-27) is shown in Fig. 3. The locations of the GNSS sites within the SAR image are shown in the same figure by black triangles. Since the phase signals from InSAR and GNSS behave similar, comparisons of the path delay from both GNSS and InSAR will be presented in section 5.

4. NEUTROSPHERIC SIGNAL IN GNSS

GNSS signals are delayed when propagating through the Earth's atmosphere. This is considered as a main limitation for high-precision geodetic applications; however, it makes GNSS a reasonable tool for atmospheric sounding, particularly in regions with highly dense networks. Fig. 1 summarises the procedures of calculating ZWD from GNSS phase observations.

The delay due to the ionosphere is eliminated by a linear combination of dual frequencies. The delay caused by the propagation through the neutrosphere, defined above as ZTD, is estimated within the GNSS data processing. PPP strategy is employed since it enables the reconstruction of absolute values of ZTD. The main interest of this work is the delay component due to water vapour (ZWD). The azimuthally isotropic part of the ZWD is calculated from the ZTD by removing the dry delay (ZDD). The anisotropic part, however, is retrieved from estimated phase residuals.

The ZDD is calculated based on an apriori empirical model presented in [11]. Given the pressure of the dry air P_0 determined at the antenna location, the ZDD can be written as:

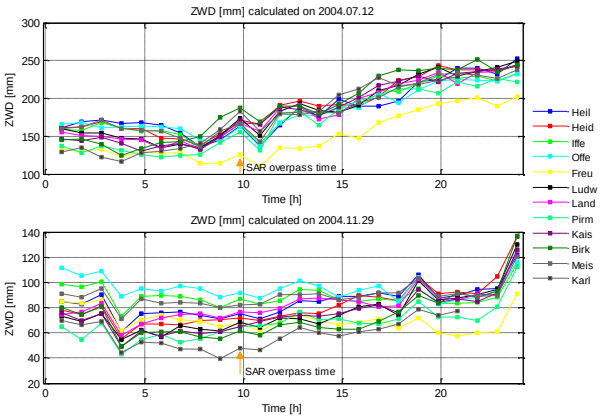

Figure 4: Time series of ZWD calculated at 12 GURN sites. The upper graph plots ZWD variations along a day in summer while the lower graph shows ZWD values along a winter day.

$$\mathrm{ZDD} = 0.002277\ \mathrm{P}_0 \cdot (1 + 0.0026 \cos 2\varphi + 0.0028\ \mathrm{H}) \quad (5)$$

where, φ is the latitude and H is the station height (km). As observed from Eq. 5, accurate quantification of the ZDD requires observations of air pressure. Interpolations of meteorological data at GNSS sites are required if the sites are not equipped with meteorological sensors.

As shown in Fig. 1, phase residuals after least squares fitting contain information about the anisotropic part of the wet delay. Consequently, site-specific error sources such as multipath (MP) and antenna phase centre variation (PCV) have to be reduced using the method proposed in [12]. The remaining part is addressed as neutrospheric delay. Time series of water vapour are determined from GPS phase observations at the days of SAR overpass. Fig. 4 shows series of SWD calculated at different GPS sites. The figure shows the change of the SWD values between summer and winter times. SWD series are consistent in the manner that they have higher values and more variations during summer.

5. WET DELAY IN INSAR AND GNSS

After the above explained processing steps are applied to the respective data set, phase delay values derived from GNSS and InSAR can be compared. Only GPS measurements are employed at this stage of the work. Bearing in mind that InSAR APS maps represent spatial variations of the temporally-differenced atmospheric phase, a similar scenario has to be applied to GNSS-based SWD series to emulate InSAR.

ZTD series are derived from GPS using observations along the day. One sample of ZTD is generated every 30 minutes. ZDD is calculated as shown in Eq. 5 and reduced to generate SWD. SWD is then mapped to the radar line-of-site by applying Eq. 3. Observing SWD over longer periods around SAR overpass enables the detection of any unexpected values of the delay.

Phase trends related to orbit inaccuracies have to be removed from InSAR data. Once this step is carried out by StaMPS, long wavelength atmospheric signals are also reduced since they are indistinguishable from orbital ramps. For that reason, a 2D linear trend is estimated and removed from the GPS data to enable a proper comparison of both data sets. Fig. 5 displays SWD as determined at GPS sites from InSAR and GPS at different radar imaging times. The SWD calculated from InSAR is averaged in a box of pixels (300×300 m^2) centred on the GPS site location. The results indicate a good agreement between SWD computed based on both systems. InSAR-based SWD differs from GPS-based SWD by an RMS of 7.14 mm. Fig. 5 exhibits also the scatter plots of the delay in InSAR vs. GPS. The correlation coefficient between the two delay sets exceeds 0.5. Thus, InSAR and GPS measurements of the neutral atmospheric delay are in a reasonable agreement.

6. CONCLUSION AND OUTLOOK

Interferometric phase images derived from repeat-pass InSAR systems show distortions most likely due to the temporal and spatial variations of atmospheric water vapour. These distortions are considered as a major limitation for Earth's topography and surface deformation studies. However, this effect can be examined for atmospheric studies. APS are extracted from InSAR interferograms by applying the technique of PSI. APS maps represent spatial variations of the path delay difference. On the other hand, GNSS enable absolute path delay assessment. This is only possible at the GNSS sites, which reduces the spatial resolution of water vapour fields derived from GNSS measurements.

A first comparison of wet delay differences quantified based on InSAR and GPS shows a good agreement between them. Further analyses are done to enlarge the understanding of the compatibility of the two systems. In this paper, cross-comparison of InSAR and GNSS in terms of the neutrospheric delay at GNSS sites was presented. Work in progress targets at evaluating APS maps from InSAR against WRF simulations of water vapour maps (which are converted into delay through Eq. 4). This is important since GNSS spatial density is limited and small-scale irregularities of water vapour cannot be observed then. Individual analyses are also done on the GNSS SWD.

The far goal of this project is the investigation of InSAR and GNSS for retrieving water vapour content. The combination of both systems is necessary since InSAR provides relative estimates of water vapour in contrary to GNSS. This research improves the understanding of the spatial variability of atmospheric turbulences over

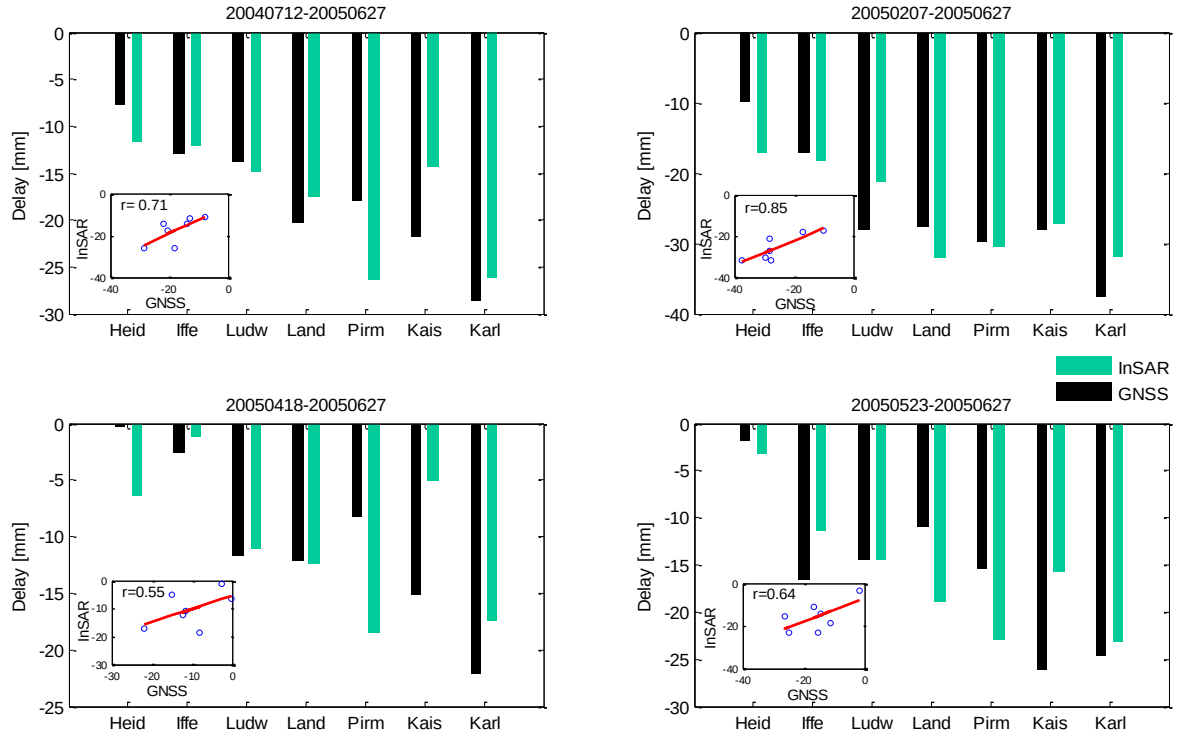

Figure 5: Path delay differences (mm) as determined from InSAR and GPS at different acquisition times. Measurements are taken over URG region. The values are compared at the GPS sites. The little figures show scatter plots of InSAR-based path delays vs. GPS-based estimates, r is the correlation coefficient.

wide scales. Observations of water vapour from InSAR and GNSS can be assimilated into numerical weather models to observe the impact on their performance.

7. ACKNOWLEDGEMENTS

The authors would like to thank ESA for providing us with ERS, ENVISAT, and MERIS data. We would like also to thank the 'Landesamt für Geoinformation und Landentwicklung Baden-Württemberg' for providing us with laser DEM data. Thanks also go to the suppliers of GNSS data: RENAG (France), RGP (France), Teria (France), Orpheon (France), SA*POS*®-Baden-Württemberg (Germany), SAPOS®-Rheinland-Pfalz (Germany), swisstopo (Switzerland), European Permanent Network, and IGS.

8. REFERENCES

[1] Bevis, M., Businger, S., Herring, T., Rocken, C., Anthes, R. & Ware, R. (1992). GPS meteorology: Remote sensing of atmospheric water vapor using the global possitioning system. *Journal of Geophysical Research* **97**, 15787–15801.

[2] MacDonald, A., Xie, Y. & Ware, R. (2002). Diagnosis of three-dimensional water vapor using slant observations from a GPS network. *Monthly Weather Review* **130,** 386–397.

[3] Hooper, A., Segall, P. & Zebker, H. (2007). Persistent scatterer InSAR for crustal deformation analysis, with application to Volc´an Alcedo, Gal´apagos. *Journal of Geophysical Research* **112** (B07407).

[4] Weather Research and Forecasting (WRF) Model: http://www.wrf-model.org/index.php

[5] Mayer, M., Knöpfler, A., Masson, F., Ulrich, P., Ferhat, G., & Heck, B. (2009). GURN (GNSS Upper Rhine Graben Network) – Research Goals and First Results of a Transnational Geo-Scientific Network. Accepted to be published by Springer in the proceedings of IAG 2009 Scientific Assembly "Geodesy for Planet Earth".

[6] Hanssen, R. (2001). *Radar Interferometry: Data Interpretation and Error Analysis*. Vol. 2, first edition, Kluwer Academic Publishers.

[7] Li, Z., Fielding, E., Cross, P. & Muller, J.-P. (2005). Interferometric Synthetic Aperture Radar (InSAR) Atmospheric Correction: GPS, Moderate Resolution Imaging Spectroradiometer (MODIS), and InSAR Integration. *Geophysical Research Letters* **110**, B03410, 2005.

[8] Onn, F. (2006). *Modeling water vapour using GPS with application to mitigating InSAR atmospheric distortions*. PhD. Dissertation, Stanford University, Stanford, California.

[9] Bevis, M., Businger, S., Chiswell, S., Herring, T. A., Anthes, R., Rocken, C. & Ware, R. H. (1994). GPS meteorology: Mapping zenith wet delays onto precipitable water. *Journal of Applied Meteorology* **33**, 379–386.

[10] Deutsch, C. & Journel, A. (1998). *GSLIB - Geostatistical Software Library and User's Guide*. Second edition, Oxford University Press, New York.

[11] Saastamoinen, J. (1972). Atmospheric correction for the troposphere and stratosphere in radio ranging of satellites, in The Use of Artificial Satellites for Geodesy, *Geophys. Monogr. Ser*., **15**, edited by S. W. Henriksen, A. Mancini, and B.H. Chovitz, 247-251, AGU, Washington, D.C.

[12] Fuhrmann, T., Knöpfler, A., Luo, X., Mayer M. & Heck, B. (2010). Zur GNSS-basierten Bestimmung des atmosphärischen Wasserdampfgehalts mittels Precise Point Positioning. KIT Scientific Reports 7561 / Schriftenreihe des Studiengangs Geodäsie und Geoinformatik 2010,2; ISBN 978-3-86644-539-0, KIT Scientific Publishing, 2010.